SLAC-PUB-9287
July 2002

Production of Charged $\pi^{\pm}$, $K^{\pm}$ and $p/\bar{p}$ in Hadronic Z^0 Decays

The SLD Collaboration[**]
Stanford Linear Accelerator Center
Stanford University, Stanford, CA 94309

ABSTRACT

We present improved measurements of identified charged hadron production at SLD, using the Cherenkov Ring Imaging Detector to identify clean samples of charged pions, kaons and protons over a wide momentum range. In addition to studying flavor-inclusive Z^0 decays, we compare the production in light, c and b flavor events, and present a new comparison of light-quark and gluon jets, selected using the SLD vertex detector. Also, we update our comparison of hadron and antihadron production in light quark (rather than antiquark) jets, selected using the high SLC electron beam polarization. Differences between hadron and antihadron production at high momentum fraction provide precise measurements of leading particle production and new, stringent tests of fragmentation models.

Contributed to the International Conference on High Energy Physics, 24–31 July, 2002, Amsterdam, The Netherlands, Ref: 970.

[*]This work was supported by Department of Energy contract DE-AC03-76SF00515.

1 Introduction

The production of final state hadrons from primary hard partons, e.g. the quark and antiquark in $e^+e^- \to Z^0 \to q\bar{q}$, is currently believed to proceed in three stages. The first stage involves the radiation of gluons from the primary quark and antiquark, which in turn radiate gluons or split into $q\bar{q}$ pairs until their virtuality approaches the hadron mass scale. Such a "parton shower" is calculable in perturbative QCD, for example in the Modified Leading Logarithm Approximation (MLLA) [1].

The second stage, in which these partons turn into "primary" hadrons, is not understood quantitatively, although several hadronization models exist. A simple model is the ansatz of Local Parton-Hadron Duality (LPHD) [1], which hypothesizes that distributions of kinematic quantities for a given hadron species are directly proportional to the parton distributions at some appropriate parton virtuality. This allows the prediction via MLLA QCD of the shapes of differential cross sections for primary hadrons, and of, for example, the energy- and mass-dependences of the peak of the distribution of $\xi = -\ln(x_p)$, where $x_p = 2p/E_{cm}$, p is the hadron momentum and E_{cm} is the e^+e^- center-of-mass energy.

The third stage, in which unstable primary hadrons decay into final state hadrons, complicates the interpretation of inclusive measurements. It is desirable to remove the effects of these decays when comparing with the predictions of QCD+LPHD. Additional complications arise in jets initiated by heavy (c or b) quarks in which the leading heavy hadrons carry a large fraction of the beam energy, restricting that available to other primary particles, and then decay into a number of secondary particles. It is thus also desirable to restrict measurements to events with light primary flavors.

Measurements of the differential cross sections of identified particles are useful for testing the predictions of QCD+LPHD and constraining models. Several such measurements have been reported in e^+e^- annihilation and QCD+LPHD has been successful in describing the shape and energy dependence of the ξ distribution for inclusive charged particles, as well as those for identified charged and neutral hadrons [2]. At a given E_{cm}, the ξ distribution for identified pions peaks at a higher value than the distributions for higher mass particle types; however little mass dependence is observed among these other species, although results for mesons and baryons are consistent with the hypothesis of separate mass dependences. It is probable that these peak positions, especially for pions, are influenced strongly by decay products of heavier particles; experimental elucidation of this issue is desirable.

A prediction of QCD is that a hard gluon will radiate more soft gluons at larger angles than a quark of equal energy, resulting an a wider jet with a higher multiplicity of softer gluons. This effect has been observed by several experiments in the multiplicity and inclusive distributions of charged tracks and energy clusters. However, there is no reason to expect any difference in the hadronization stage, so that the relative production of different particle species should be the same in gluon jets as in light quark jets. There are currently few measurements in this area, with limited precision.

A particularly interesting aspect of jet fragmentation is the question of what happens to the primary quark or antiquark that initiated the jet. Many fragmentation models assume that the initial quark is "contained" as a valence constituent of a particular hadron, and that this "leading" hadron has on average a higher momentum than the other particles in the jet. This phenomenon has not been studied precisely for high-energy light-flavor jets, since it is difficult to identify the sign and flavor of the initial $q/\bar{q}$ on a jet-by-jet basis. The quantification of leading particle effects could lead to ways to identify the primary flavor of arbitrary samples of jets, enabling a number of new measurements in e^+e^-, as well as in ep and p$\bar{\text{p}}$, collisions.

Here we present an analysis of $\pi^\pm$, $K^\pm$, and p/$\bar{\text{p}}$ production in hadronic Z^0 decays collected by the SLC Large Detector (SLD), based upon the sample of 450,000 hadronic events obtained in runs of the SLAC Linear Collider (SLC) between 1996 and 1998. We update our measurements of differential cross sections in an inclusive sample of hadronic events of all flavors, and also in high-purity samples of light- ($Z^0 \to u\bar{u}, d\bar{d}, s\bar{s}$), c- ($Z^0 \to c\bar{c}$) and b-flavor ($Z^0 \to b\bar{b}$) events. The unfolded differential cross sections for the light-flavor events are free from effects of heavy quark production and decay, and as such provide a more appropriate sample for comparison with QCD predictions, which generally assume massless quarks, although the influence of decay products of other unstable primary hadrons remains. We use these measurements to test the predictions of MLLA QCD+LPHD and of various fragmentation models.

In addition, we tag a high-purity sample of gluon jets in 3-jet events, and compare the production with light quark jets of the the same energy, in order to test the universality of the hadronization process. We also select samples of quark and antiquark jets from our light-flavor event sample, using the large forward-backward production asymmetry in polar angle inherent in collisions of highly polarized electrons with positrons. The differential cross sections are measured separately for hadrons and antihadrons in light-quark jets, and the observed differences are interpreted in terms of leading particle effects. These measurements provide precise, unique tests of fragmentation models.

2 The SLD and Hadronic Event Selection

A description of the SLD can be found in Ref. [3]; the trigger and initial selection criteria for hadronic Z^0 decays are described in Ref. [4]. This analysis used charged tracks measured in the Central Drift Chamber (CDC) [5] and Vertex Detector (VXD) [6], and identified using the Cherenkov Ring Imaging Detector (CRID) [7]. Momentum measurement is provided by a uniform axial magnetic field of 0.6T. The CDC and VXD give a momentum resolution of $\sigma_{p_\perp}/p_\perp = 0.01 \oplus 0.0026 p_\perp$, where $p_\perp$ is the track momentum transverse to the beam axis in GeV/c. In the plane normal to the beamline the centroid of the micron-sized SLC interaction region was reconstructed from tracks in sets of approximately thirty sequential hadronic Z^0 decays to a precision of $\sigma_{IP} \simeq 3$ μm and used as an estimate of the primary interaction point (IP). The IP position along

the beam axis was determined event by event using charged tracks, with an average resolution of $\sigma_{IP}^{z} \simeq 20$ μm. Including the uncertainty on the IP position, the resolution on the charged track impact parameter (δ) was parametrized in the plane perpendicular to the beamline as $\sigma_{\delta}^{r\phi}$ =8$\oplus$29/($p \sin^{3/2}\theta$) μm, and in any plane containing the beam axis as σ_{δ}^{z} =9$\oplus$29/($p \sin^{3/2}\theta$) μm, where θ is the track polar angle with respect to the beamline. The CRID comprises two radiator systems that allow the identification of charged pions with high efficiency and purity in the momentum range 0.3–35 GeV/c, charged kaons in the ranges 0.75–6 GeV/c and 9–35 GeV/c, and protons in the ranges 0.75–6 GeV/c and 10–46 GeV/c [8]. The event thrust axis [9] was calculated using energy clusters measured in the Liquid Argon Calorimeter [10].

A set of cuts was applied to the data to select well-measured tracks and events well contained within the detector acceptance. Charged tracks were required to have a point of closest approach to the beam axis within 5 cm transverse, and within 10 cm along the axis from the measured IP, as well as $|\cos\theta| < 0.80$, and $p_{\perp} > 0.15$ GeV/c. Events were required to have a minimum of five such tracks, a thrust axis polar angle w.r.t. the beamline, θ_T, within $|\cos\theta_T| < 0.71$, and a charged visible energy E_{vis} of at least 20 GeV, which was calculated from the selected tracks assigned the charged pion mass. The efficiency for selecting a well-contained $Z^0 \to q\bar{q}(g)$ event was estimated to be above 96% independent of quark flavor. The VXD, CDC and CRID were required to be operational, resulting in a selected sample of roughly 288,000 events, with an estimated non-hadronic background contribution of $0.30 \pm 0.01\%$ dominated by $Z^0 \to \tau^+\tau^-$ events.

Samples of events enriched in light, c, and b primary flavors were selected using tracks with well measured impact parameters δ with respect to the IP. For each event we define n_{sig}^{evt} as the number of tracks with impact parameter greater than three times its estimated error, $\delta > 3\sigma_{\delta}$. We also run a topological vertex finding algorithm [11] on the set of tracks in each hemisphere and consider the p_t-corrected mass M_{pt} of any vertex found. Any event containing a vertex with $M_{pt} > 2$ GeV/c^2 was assigned to the b-tagged sample; an event without such a vertex, but having either $n_{sig} > 2$ or a vertex with $M_{pt} > 0.5$ GeV/c^2, $p_{vtx} > 2$ GeV/c and $p_{vtx} - 14M_{pt} > -10$ was assigned to the c-tagged sample; events with no found vertices and $n_{sig} = 0$ were assigned to the light flavor sample. The light, c and b samples comprised 101,000, 34,000 and 40,000 events, respectively; selection efficiencies and sample purities were estimated from our Monte Carlo simulation and are listed in table 1.

A sample of gluon jets was selected from 3-jet events, defined by applying the Durham jetfinding algorithm to the set of charged tracks in the event with a resolution parameter of $y_{cut} = 0.005$. This algorithm and y_{cut} value were chosen to minimize the migration of tracks from heavy hadron decays into the wrong jet. The jets energies were rescaled using massless kinematics and the two lower energy jets were considered as gluon candidates if the angle between their axes exceeded 20 degrees. The topological vertex finder was run on the set of vertex quality tracks in each jet and the n_{sig}^{jet} was calculated for each jet. If a vertex with $M_{pt} > 0.75$ GeV/c^2 and $p_{vtx} > 3$ GeV/c was

	Efficiency for $Z^0 \rightarrow$			Purity of $Z^0 \rightarrow$		
	$u\bar{u}, d\bar{d}, s\bar{s}$	$c\bar{c}$	$b\bar{b}$	$u\bar{u}, d\bar{d}, s\bar{s}$	$c\bar{c}$	$b\bar{b}$
light-tag	0.734	0.190	0.010	0.928	0.068	0.004
c-tag	0.049	0.551	0.105	0.203	0.641	0.156
b-tag	0.001	0.024	0.815	0.005	0.023	0.972

Table 1: Tagging efficiencies for simulated events in the three flavor categories to be tagged as light, c or b. The three rightmost columns indicate the composition of each simulated tagged sample assuming SM relative flavor production.

found in one of the two lower energy jets, then the other was tagged as a gluon jet if it contained no vertex, had an energy greater than 3 GeV and the polar angle of its axis satisfied $|\cos\theta_{jet}| < 0.7$. This results in 12,290 jets tagged with an estimated 92% gluon purity. The distribution of tagged gluon jet energy is shown in fig. 1; the simulation is consistent with the data and the background contributions are indicated, the dominant source being $b/\bar{b}$ jets. We compare with a light-mixture sample, comprising any of the two lowest energy jets in 3-jet events tagged as light-flavor, as described above, with an axis satisfying $|\cos\theta_{jet}| < 0.7$. This sample is estimated to be 46% true gluon jets and 48% light quark jets, with a small background from c and b jets, however the light quark fraction varies strongly with jet energy, from about one-fourth at $E_{jet} \approx$10 GeV to about three-fourths at $E_{jet} \approx$35 GeV. As cross-checks we also consider a b-mixture and a c-mixture, defined as the two lowest energy jets in events in which the highest energy jet contained a b or c vertex (see above), respectively.

Separate samples of hemispheres enriched in light-quark and light-antiquark jets were selected by exploiting the large electroweak forward-backward production asymmetry wrt the beam direction. We first applied a looser light-flavor tag, requiring only that $n_{sig}^{evt} = 0$. The event thrust axis was used to approximate the initial $q\bar{q}$ axis and was signed such that its z-component was positive, $\hat{t}_z > 0$. Events in the central region of the detector, where the production asymmetry is small, were removed by the requirement $|\hat{t}_z| > 0.15$, leaving 190,000 events. The quark-tagged hemisphere in events with left-(right-)handed electron beam was defined to comprise the set of tracks with positive (negative) momentum projection along the signed thrust axis. The remaining tracks in each event were defined to be in the antiquark-tagged hemisphere. The sign and magnitude of the electron beam polarization were measured for every event. For the selected event sample, the average magnitude of the polarization was 0.73. Using this value and assuming Standard Model couplings at tree-level, the purity of the quark-tagged sample is 0.73.

For the purpose of estimating the efficiency and purity of the event flavor tagging and the particle identification, we made use of a detailed Monte Carlo (MC) simulation of the detector. The JETSET 7.4 [12] event generator was used, with parameter

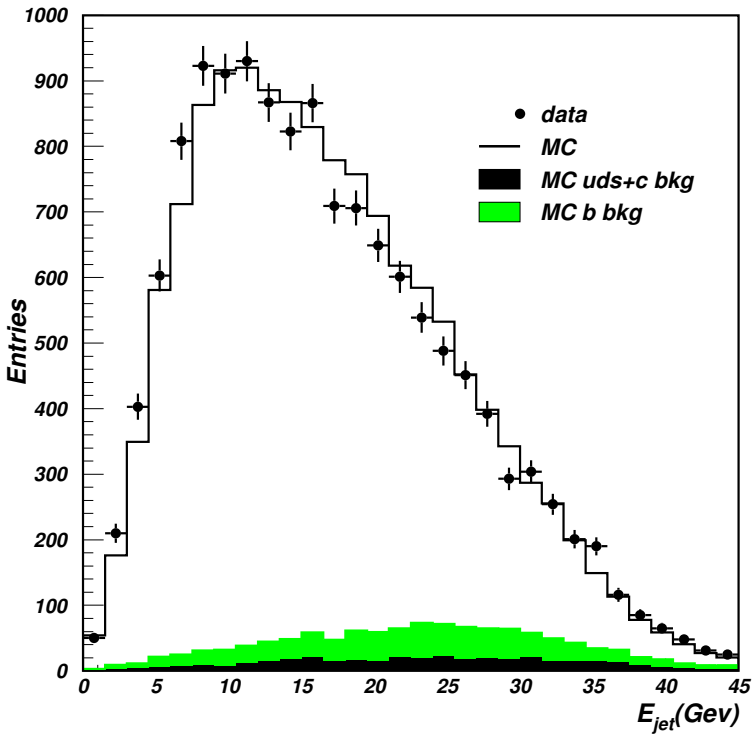

Figure 1: Distribution of the reconstructed energies of the tagged gluon jets in the data (dots) and simulation (histogram). The simulated contributions from non gluon jets are indicated.

values tuned to hadronic e^+e^- annihilation data [13], combined with a simulation of B-hadron decays tuned [14] to $\Upsilon(4S)$ data and a simulation of the SLD based on GEANT 3.21 [15]. Inclusive distributions of single-particle and event-topology observables in hadronic events were found to be well described by the simulation [4].

3 Measurement of the Charged Hadron Fractions

Charged tracks were identified as pions, kaons or protons in the CRID using a likelihood technique [16]. Information from the liquid (gas) radiator only was used for tracks with $p < 2.25$ ($p > 9.5$) GeV/c; in the overlap region, $2.25 < p < 9.5$ GeV/c, liquid and gas information was combined. Additional track selection cuts were applied to remove tracks that scattered through large angles before exiting the CRID and to ensure that the CRID performance was well-modelled by the simulation. Tracks were required to have at least 40 CDC hits, at least one of which was in the outermost superlayer, to extrapolate through an active region of the appropriate radiator(s), and to have at least 50% of their expected liquid and/or gas ring contained within a sensitive region of the CRID TPCs. The latter requirement included rejection of tracks with $p > 2.25$ GeV/c for which there was a saturated CRID hit (from passage of miminum-ionizing particles) within a 2.0 cm radius of the expected gas ring center (the maximum ring

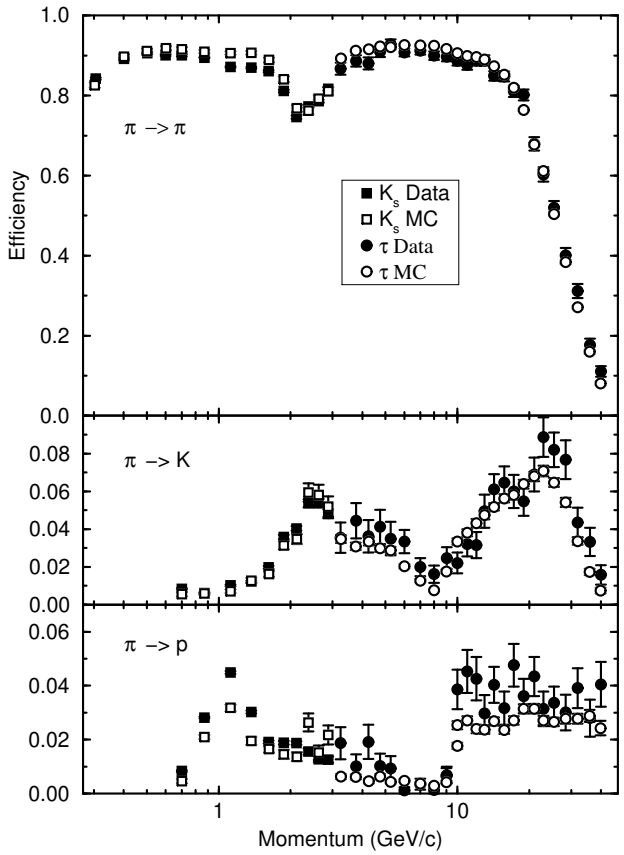

Figure 2: Calibration of the pion identification efficiencies using tracks from tagged K_s^0 and $\tau^{\pm}$ decays.

radius is ~2.5 cm). Tracks with $p < 9.5$ GeV/c that extrapolated through an active TPC were required to have a saturated hit in that TPC within 1 cm of the extrapolated track; tracks with $p > 2.25$ GeV/c were required to have either such a saturated hit or the presence of at least four hits consistent with a liquid ring. These cuts accepted 82, 70 and 77% of tracks within the barrel acceptance in the momentum ranges $p < 2.25$, $2.25 < p < 9.5$ and $p > 9.5$ GeV/c, respectively.

For tracks with $p < 2.25$ ($p > 2.25$) GeV/c, we define a particle to be identified as type j, where $j = \pi, K$,p, if $\mathcal{L}_j$ exceeds both of the other log-likelihoods by at least 3 (2) units. Efficiencies for identifying selected particles of true type i as type j were determined where possible from the data, using tracks from tagged K_s^0, $\tau^{\pm}$, ϕ and Λ^0 decays, as described in [8]. An example is shown in fig. 2. A detailed Monte Carlo (MC) simulation of the detector was then used to make small corrections to these measurements, and to derive the remaining efficiencies from those measured. These efficiencies are parametrized in terms of continuous functions in each of the three momentum ranges, and are shown in fig. 3, in which the pairs of lines represent our estimated efficiencies plus and minus their systematic uncertainties. These uncertainties correspond to the statistical errors on the ratios of parameters fitted to the data

and MC calibration samples, and are strongly positively correlated across each of the three momentum regions. The diagonal elements peak near or above 0.9 and the pion coverage is continuous from 0.3 GeV/c up to near the beam momentum. There is no kaon-proton separation below 0.75 GeV/c since both particles are below Cherenkov threshold in the liquid system; it is also poor between 7 and 10 GeV/c due to the limited resolution of the liquid system and the fact that both particles are below threshold in the gas system. The proton (kaon) coverage extends well beyond (to nearly) the beam momentum. Misidentification rates are typically less than 0.04, with peak values of up to 0.1.

In each momentum bin we measured the fractions of the selected tracks that were identified as π, K and p. The observed fractions were related to the true production fractions by an efficiency matrix, composed of the values in fig. 3 for that bin. This matrix was inverted and used to unfold our observed identified particle rates. This analysis procedure does not require that the sum of the charged particle fractions be unity; instead the sum was used as a consistency check and was found to be within errors of unity for all momenta. At very low momentum, where we cannot distinguish kaons from protons, the procedure was reduced to a 2×2 matrix analysis and we present only the pion fraction.

Electrons and muons were not distinguished from pions in this analysis; this background was estimated from the simulation to be about 5% in the inclusive flavor sample, predominantly from c- and b-flavor events. The flavor-inclusive fractions were corrected using the simulation for the lepton backgrounds, as well as for the effects of beam-related backgrounds, particles interacting in the detector material, and particles with large flight distance, such that the conventional definition of a final-state charged hadron is recovered, namely charged pions, kaons or protons that are either from the primary interaction or decay products of particles with lifetime less than 3×10^{-10}s.

The measured charged particle fractions for inclusive hadronic Z^0 decays are shown in fig. 4. The errors on the points below about 15 GeV/c are dominated by the systematic uncertainties on the identification efficiencies and are strongly positively correlated. For $p > 15$ GeV/c the systematic errors are again positively correlated and increase with momentum, however the statistical errors increase more rapidly, and dominate for momenta above about 20 GeV/c.

Pions are seen to dominate the charged hadron production at low momentum, and to decline steadily in fraction as momentum increases. The kaon fraction rises steadily with momentum, and the proton fraction rises to a maximum of about one-tenth at about 15 GeV/c, then declines slowly. At high x_p, the pion and kaon fractions appear to be converging. This convergence could indicate reduced strangeness suppression at high momentum, or that production is becoming dominated by leading particles, such that kaons from $s\bar{s}$ events are as common as pions from $u\bar{u}$ and $d\bar{d}$ events. Where the momentum coverage overlaps, these measured fractions were found to be in agreement with our previous results [8] and with other measurements at the Z^0 [17, 18, 19]. Measurements based on ring imaging [8, 17] and those based on ionization energy loss

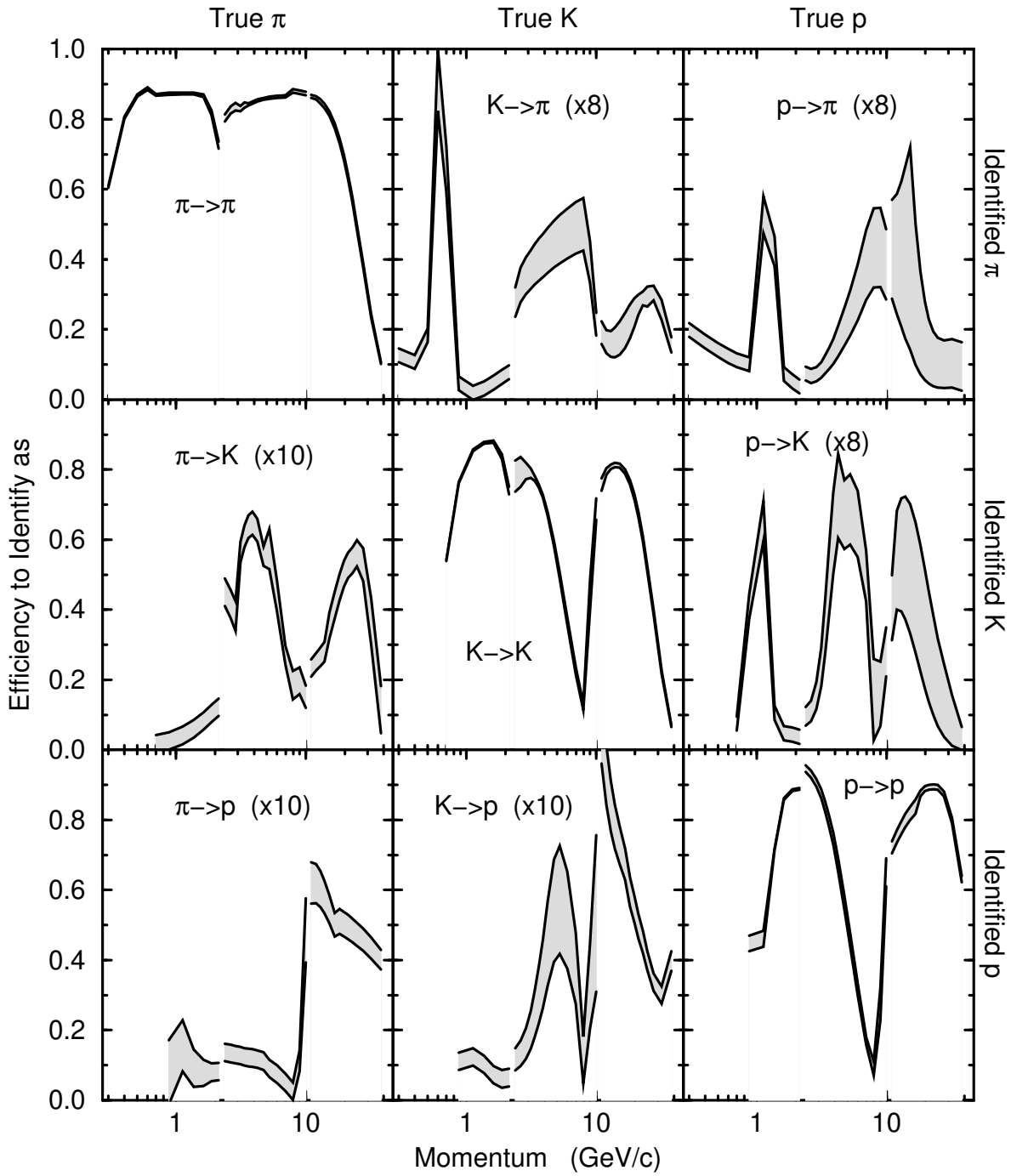

Figure 3: Calibrated identification efficiencies for tracks used in the charged hadron fractions analysis. The separations between the pairs of lines represent the systematic uncertainties, which are strongly correlated between momenta.

rates [18, 19] cover complementary momentum ranges and can be combined to provide continuous coverage over the range $0.2 < p < 46$ GeV/c.

Also shown in fig. 4 are the predictions of the JETSET 7.4 [12], UCLA [20] and HERWIG 5.8 [21] fragmentation models, using default parameters. The momentum dependence of each fraction is reproduced qualitatively by all three models. The JETSET prediction for the pion fraction is low for $1< p <4$ GeV/c, and the HERWIG and UCLA predictions are high for $4< p <20$ GeV/c; none of these models describes the data well at very high p. All three predictions for the kaon fraction are too high (low) at small (large) p. The JETSET prediction for the proton fraction is too high for all $p >2$ GeV/c; those of HERWIG and UCLA show structure in the proton fraction at large p that is inconsistent with the data.

Differential production cross-sections were obtained by multiplying these fractions by our measured inclusive charged hadron differential cross section. Figure 5 shows our measured differential cross sections per hadronic event of these three hadron species, along with our previous results for the K^0, K^{*0}, ϕ and Λ. We confirm the roughly 10% higher production of charged than neutral kaons at intermediate momenta.

Figure 6 the same differential cross sections for the three charged hadron species as a function of the variable $\xi = -\ln x_p$. Calculations using the modified leading logarithm approximation (MLLA) predict that the distribution of ξ for partons in a parton shower evolved down to a virtuality scale Q_0 should have a shape that is well approximated by a Gaussian distribution within $\sim$1 unit of the peak, and approximated by a slightly distorted Gaussian over a wider range. The ansatz of LPHD requires that the spectrum of directly produced hadrons have this same form, and that the position of the peak of the distribution for a given hadron species depend on the hadron mass and the c.m. energy.

Also shown in fig. 6 are the results of Gaussian fits over the largest range about the peak over which a good fit could be obtained. We find that the simple Gaussian function provides a good description of our data over a range of roughly ± 1 unit of ξ around the peak position. The peak position ξ^* for each particle type was taken to be the mean value of the fitted Gaussian. Systematic errors were evaluated by varying the fit range and applying correlated experimental systematic errors. We find

$$\begin{aligned} \xi^*_\pi &= 3.77 \pm 0.01 \pm 0.02 \\ \xi^*_K &= 2.63 \pm 0.01 \pm 0.03 \\ \xi^*_{\mathrm{p}} &= 2.94 \pm 0.02 \pm 0.06, \end{aligned}$$

where the first error is statistical and the second systematic. We also fitted Gaussians with the addition of a skewness term, and found that the fittable range could be extended toward lower values of ξ but not higher values. Also adding a kurtosis term, we could describe the data over essentially the full measured range of ξ. The fit corresponding to the widest range that gave a χ^2 value less than twice the number of degrees of freedom is shown in fig. 6.

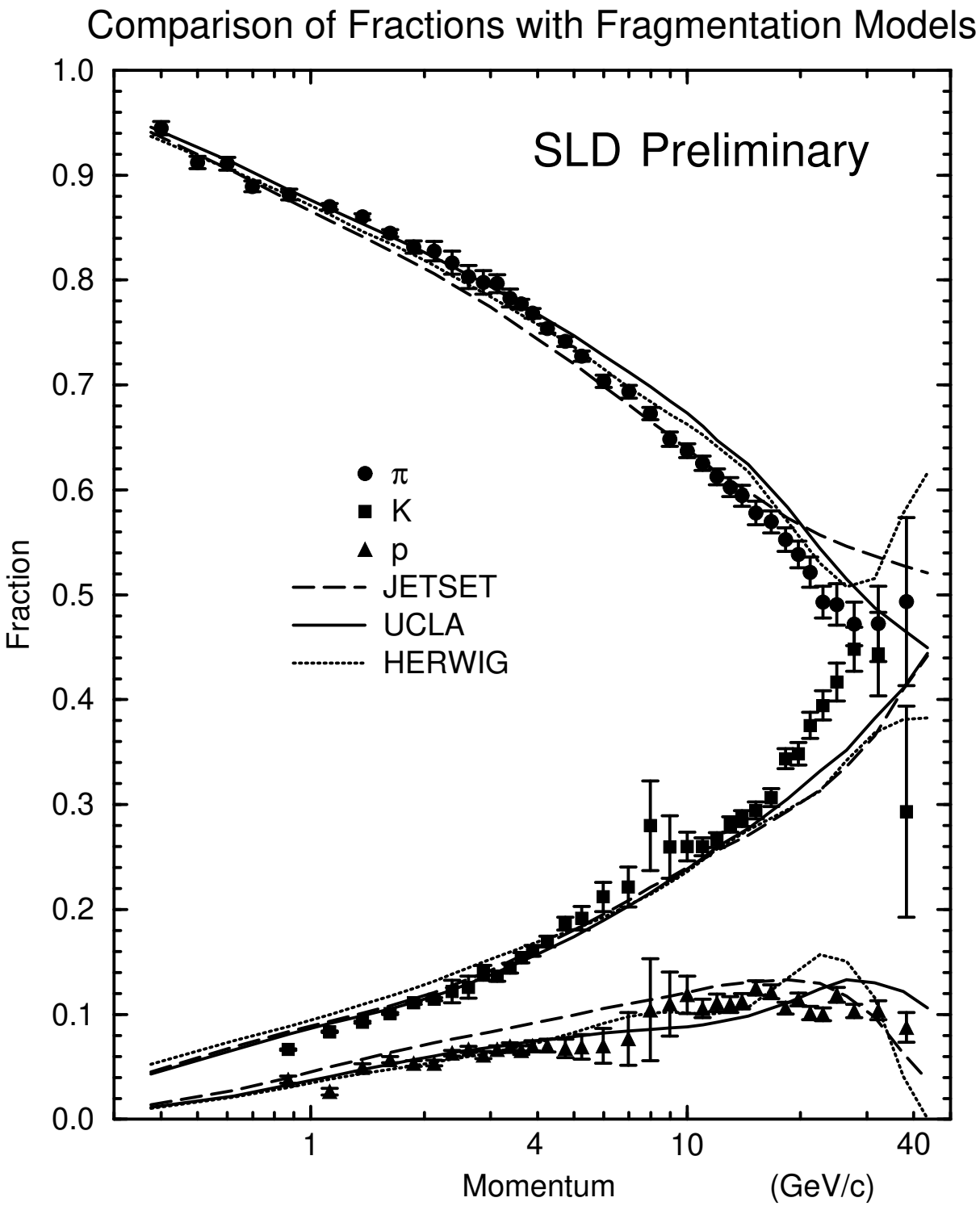

Figure 4: Comparison of the charged hadron fractions in flavor-inclusive events with the predictions of three fragmentation models.

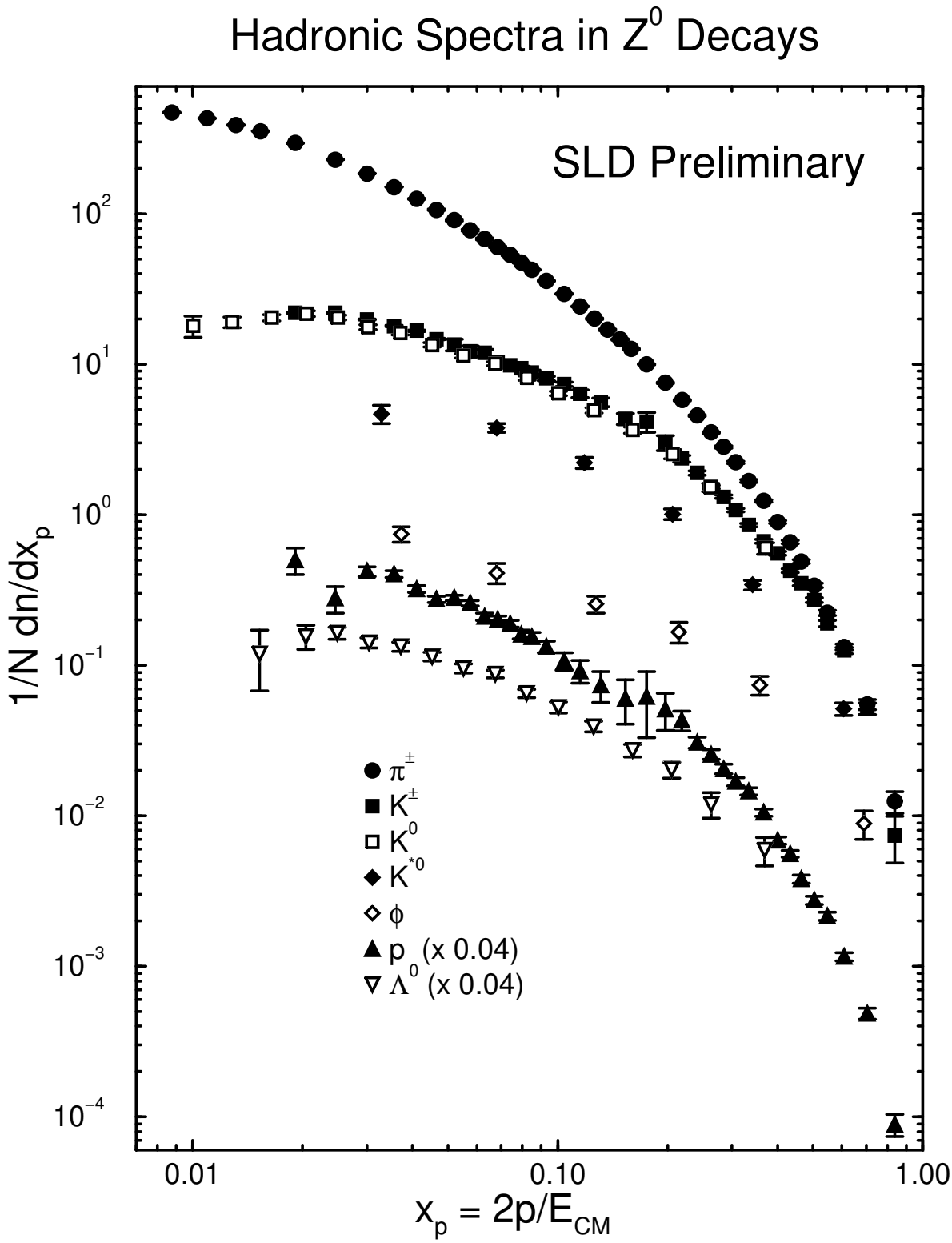

Figure 5: Measured production of seven identified particle species in hadronic Z^0 decays. Results for the neutral hadrons are from Ref. [8].

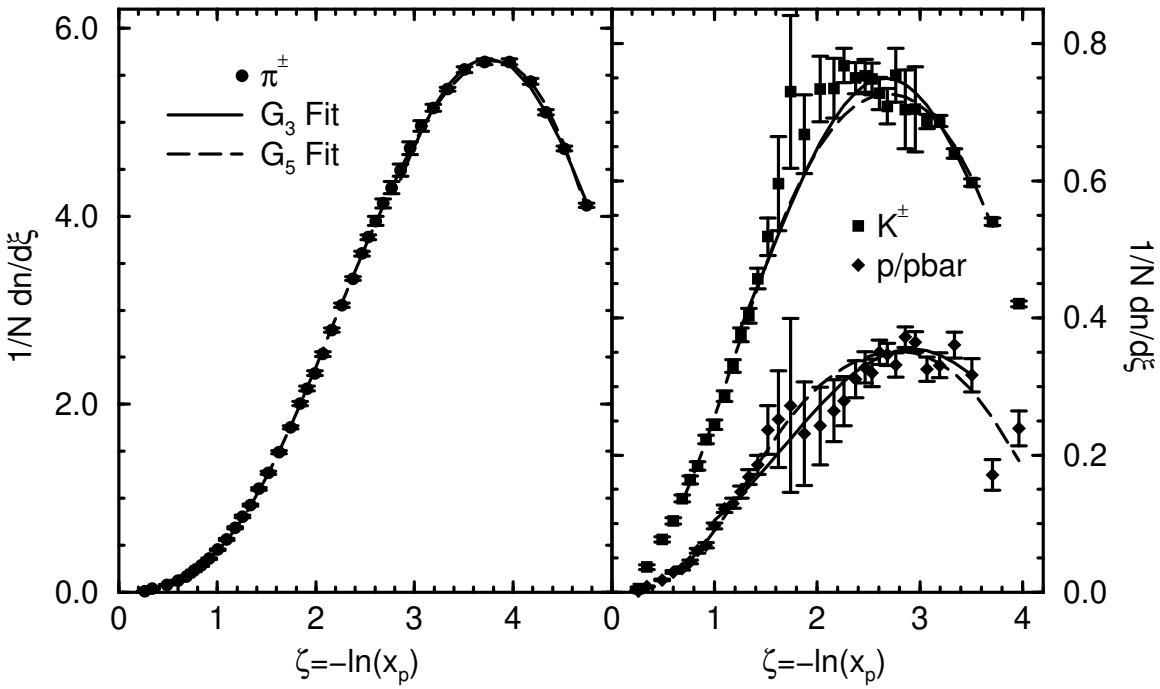

Figure 6: Measured differential cross sections per hadronic event per unit $\xi = -\ln x_p$ for the production of charged pions (left), kaons (squares) and protons (diamonds). The (dashed) lines are the results of Gaussian (plus skewness and kurtosis terms) fits over the ranges indicated by the extents of the lines.

4 Flavor-Dependent Analysis

The analysis was repeated separately on the high-purity light-, c and b-tagged event samples described in section 2. In each momentum bin the measured differential cross sections r_j^{meas} of each hadron species for these three samples, j =light-tag, c-tag, b-tag, were unfolded by inverting the relations:

$$r_j^{meas} = \frac{\Sigma_i b_{ij} \epsilon_{ij} R_i r_i^{true}}{\Sigma_i \epsilon_{ij} R_i} \tag{1}$$

to yield true differential cross sections r_i^{true} in events of the three flavor types, i =1, 2, 3, corresponding to $Z^0 \to u\bar{u}, d\bar{d}, s\bar{s}$, $Z^0 \to c\bar{c}$ and $Z^0 \to b\bar{b}$. Here, R_i is the fraction of hadronic Z^0 decays of flavor type i, taken from [22], ϵ_{ij} is the event tagging efficiency matrix, estimated from the simulation and listed in table 1, and b_{ij} represents the momentum-dependent bias of tag j toward selecting events of flavor i that contain hadrons of the type in question. The diagonal bias values [23] are within a few percent of unity, reflecting a small multiplicity dependence of the flavor tags. The off-diagonal bias values are larger, but these have little effect on the unfolded results.

Our measured charged hadron fractions in light-flavor flavor events show qualitative behaviour quite similar those in the flavor-inclusive sample, however these are more relevant for comparison with QCD predictions based on the assumption of massless

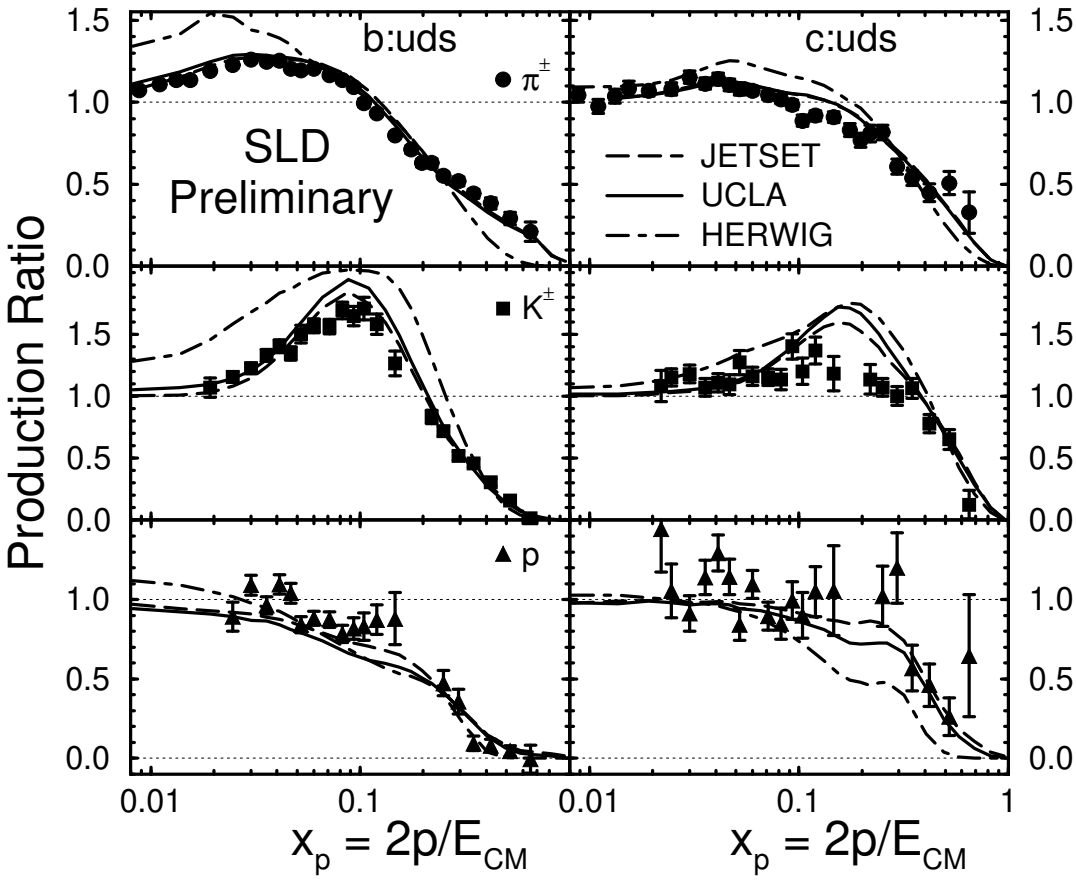

Figure 7: Ratios of production rates in b-flavor events to those in light-flavor events, along with the predictions of three fragmentation models.

primary quark production, as well as for determining parameters in fragmentation models. We observe the same general differences between the predictions of the three fragmentation models and the data as were seen above, indicating that these deficiencies are in the fragmentation simulation and not simply in the modelling of heavy hadron production and decay.

In fig. 7 we show the ratios of production in b- to light-flavor and c- to light-flavor events for the three species. The systematic errors on the particle identification largely cancel in these ratios, and the resulting errors are predominantly statistical. There is greater production of charged pions in b-flavor events at low momentum, with an approximately constant ratio for $0.02 < x_p < 0.07$. The production charged kaons is approximately equal in the two samples at $x_p = 0.02$, but the relative production in b-flavor events then increases with x_p, peaking at $x_p \approx 0.07$. There is approximately equal production of protons in b-flavor and light-flavor events below $x_p = 0.15$. For $x_p > 0.1$, production of all these particle species falls faster with increasing momentum in b-flavor events. These features are consistent with expectations based on the known properties of $Z^0 \to b\bar{b}$ events, namely that a large fraction of the event energy is carried by the leading B- and $\bar{B}$-hadrons, which decay into a large number of lighter particles. Also shown in fig. 7 are the predictions of the three fragmentation models, which reproduce these features qualitatively, although HERWIG overestimates the pion and

kaon ratios by a large factor at low x_p.

There is higher kaon production in c-flavor events than in light-flavor events at $x_p \sim 0.1$, reflecting the tendency of c-jets to produce a fairly hard charmed hadron whose decay products include a kaon carrying a large fraction of its momentum. There are fewer additional charged pions produced in D decays than in B decays, so that pion production is only slightly higher in c-flavor events at very small x_p. The pion c:light ratio starts to cut off at a larger value, $x_p \approx 0.3$, than the corresponding b:light ratio, attributable to the lower average decay multiplicity and softer fragmentation function of D hadrons, and the kaon and proton ratios are consistent with this cutoff point. Again, all three fragmentation models reproduce the data qualitatively, although HERWIG overestimates the pion ratio at small x_p, as it did in the b:light case, and underestimates the proton ratio is large x_p.

5 Relative Production in Gluon Jets

The fractions analysis was then repeated on the high-purity gluon jet sample described in section 2, as well as on the light-, c- and b-mixture samples. The results for the latter two samples were found to be consistent with the predictions of the simulation, indicating that the small c and b jet backgrounds in both the gluon-tagged and light-misture samples are well modelled.

As a first comparison, we show in fig. 8 the ratio of the pion fraction measured in the gluon-tagged sample to that measured in the light-mixture sample, along with the corresponding ratios for kaons and protons. There are significant deviations from unity in these ratios, however they are reproduced by our simulation, so can be explained as kinematic biases due, for example, to the different average jet energy in the gluon-tagged and light-mixture samples. We thus conclude that at the level of our errors of a few percent, the relative production properties of charged pions, kaons and protons are the same.

6 Leading Particle Effects

We extended [24] these studies to look for differences between particle and antiparticle production in quark (rather than antiquark) jets, in order to address the question of whether e.g. a primary u-initiated jet contains more particles that contain a valence u-quark (e.g. π^+, K^+, p) than particles that do not (e.g. π^-, K^-, $\bar{\mathrm{p}}$). To this end we used the light quark- and antiquark-tagged hemispheres described in section 2.

We measured the production rates per light quark jet

$$R_h^q = \frac{1}{2N_{evts}} \frac{d}{dx_p} \left[N(q \to h) + N(\bar{q} \to \bar{h}) \right], \tag{2}$$

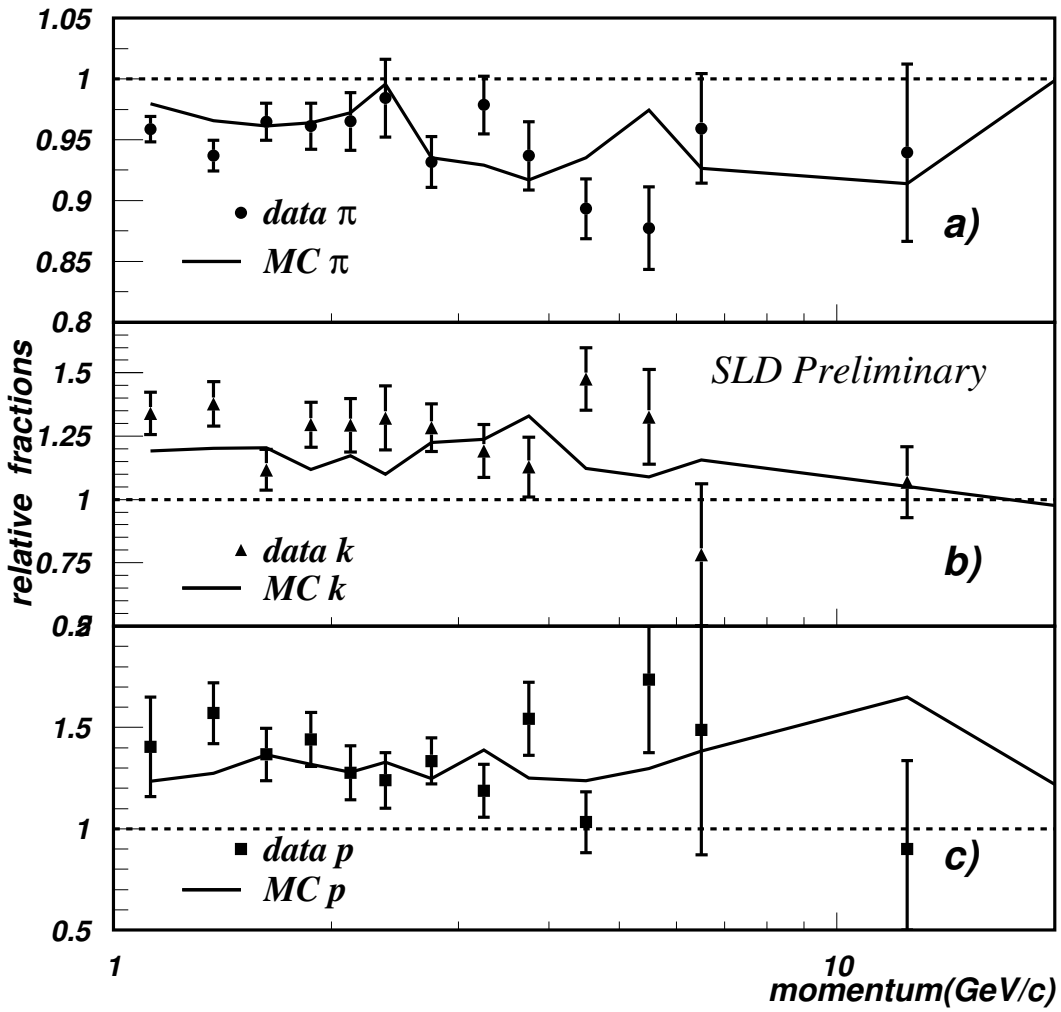

Figure 8: Ratios of fractions in g-tagged jets to those in light-mixture jets, along with the predictions of our simulation.

$$R^q_{\bar{h}} \;=\; \frac{1}{2N_{evts}}\frac{d}{dx_p}\left[N(q\to\bar{h})+N(\bar{q}\to h)\right], \tag{3}$$

where: q and $\bar{q}$ represent light-flavor quark and antiquark jets respectively; N_{evts} is the total number of events in the sample; h represents any of the identified hadrons π^-, K^-, and p, and $\bar{h}$ indicates the corresponding antiparticle. Then, for example, $N(q\to h)$ is the number of hadrons of type h in light quark jets.

The charged hadron fractions analysis was repeated separately on the positively and negatively charged tracks in each of the quark- and antiquark-tagged samples. Results for the positively charged tracks in the quark-tagged sample and the negatively-charged tracks in the antiquark-tagged sample were consistent, so these two samples were combined and labelled as positively charged hadrons from light quark jets, yielding measured values of $R^q_{\pi^+}$, $R^q_{K^+}$, and $R^q_{\rm p}$ in the tagged samples. The same procedure applied to the remaining tracks yielded $R^q_{\pi^-}$, $R^q_{K^-}$, and $R^q_{\bar{\rm p}}$.

It is essential to understand the contributions to these rates from heavy-flavor events, which are typically large in the momentum range we cover and show substantial differences between hadron and antihadron due to decay products of the heavy hadrons. This motivated our use of light-tagged events, and the residual heavy flavor contributions were estimated from the simulation to be typically 15% of the observed hadrons. This estimate was applied as a correction, yielding differential cross sections per light-quark-tagged jet. The effect of this correction on the results was negligible compared with the statistical errors.

For each hadron type, differential cross sections in light quark jets were then extracted by correcting for the light-tag bias and unfolding for the effective quark (vs. antiquark) purity. The purity was estimated from the simulation to be 0.72, which is slightly lower than the value of 0.73 noted in section 2, reflecting the cutoff in acceptance of the barrel CRID at $|\cos\theta| = 0.68$.

The measured differential cross sections per light quark jet are shown in fig. 9. The errors shown are are the sum in quadrature of statistical errors and those systematic errors arising from uncertainties in the heavy-flavor background correction and the effective quark purity; the statistical errors dominate this total. Systematic errors common to hadron and antihadron, such as those due to their identification efficiencies, are not included.

In all cases the hadron and antihadron differential cross sections are consistent at low x_p. Significant differences appear at $x_p \approx 0.3$, 0.1 and 0.25 for charged pions, kaons and protons, respectively, and increase with increasing x_p. At the highest momenta protons dominate over antiprotons and K^- over K^+. It is convenient to show these data in the form of the difference between hadron and antihadron differential cross sections normalized by the sum:

$$D_h = \frac{R_h^q - R_{\bar{h}}^q}{R_h^q + R_{\bar{h}}^q}, \tag{4}$$

The common systematic errors cancel explicitly in this variable. Results are shown in fig. 10, along with our previous [8] similar results for the strange vector meson K^{*0} and the Λ^0 hyperon. A value of zero corresponds to equal production of hadron and antihadron, and the data are consistent with zero at low x_p. A value of $+1$ (-1) corresponds to complete dominance of (anti)hadrons h.

The baryon results are most straightforward to interpret. Since baryons contain valence quarks and not antiquarks, the excess of baryons over antibaryons in light quarks jets provides clear evidence for the production of leading baryons at high scaled momentum. The data suggest that the effect begins at $x_p \approx 0.2$ and are consistent with both a steady increase with x_p and a rise to a plateau of $D_{\rm p} \approx 0.4$.

The interpretation for the mesons is more complicated, since they contain one valence quark along with one antiquark. All down-type quarks are produced equally and with the same SM forward-backward asymmetry in Z^0 decays, so that if a leading neutral particle such as K^{*0} ($d\bar{s}$) were produced equally in d and $\bar{s}$ jets then one

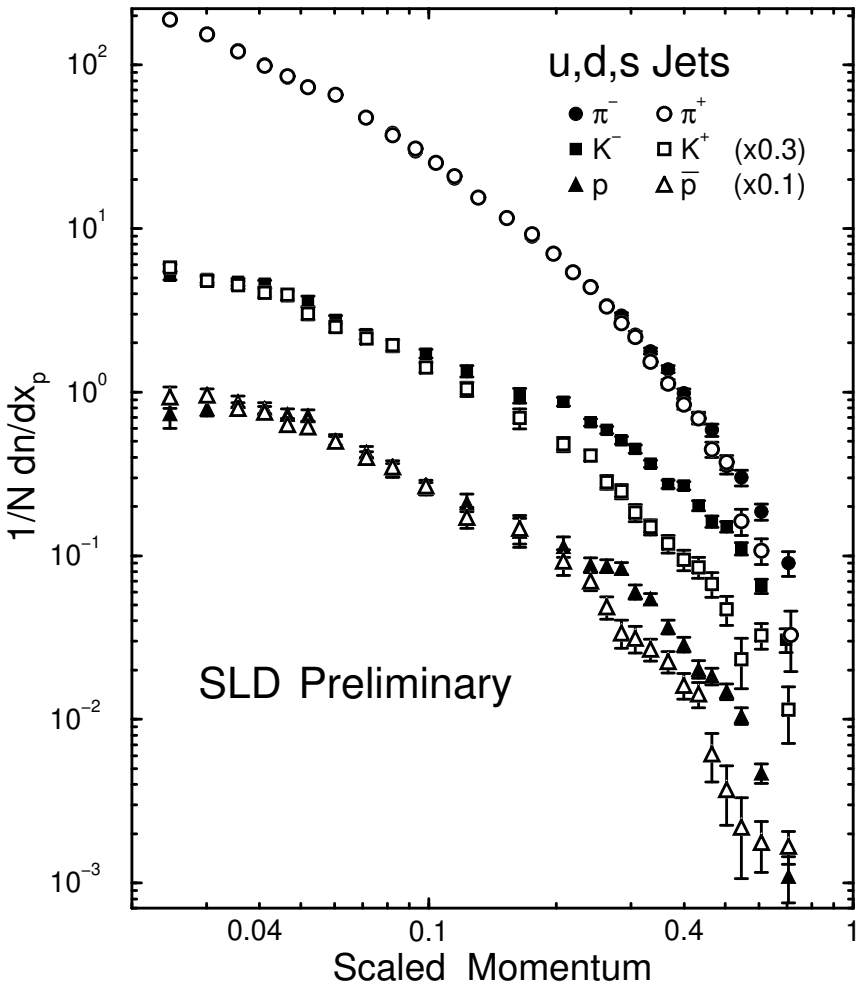

Figure 9: Scaled momentum distributions of identified particles and their antiparticles per light quark (u, d, s) jet.

would observe $D_{\overline{K}^{*0}} = 0$. In the case of charged mesons such as π^- ($d\bar{u}$), the different production rates and forward-backward asymmetries of up- and down-type quarks cause a nonzero dilution of leading particle effects. At the Z^0, equal leading pion production in u- and d-jets would lead to a dilution factor of 0.27.

Our measured D_{π^-} are significantly above zero at high x_p, and consistent with $0.27 D_{\rm p}$. Thus leading primary pions are produced in light quark jets with a relative fraction similar to that for baryons at high momentum. The onset of the effect is at a much higher value of x_p, perhaps due to a large "background" contribution from decays of ρ^0, K^*, etc. Our measured D_{K^-} are well above both zero and $0.27 D_{\rm p}$ for $x_p > 0.1$. This indicates both substantial production of leading $K^\pm$ mesons at high momentum, and a depletion of leading kaon production in $u\bar{u}$ and $d\bar{d}$ events relative to $s\bar{s}$ events.

Assuming these high-momentum kaons to be directly produced in the fragmentation process, this amounts to a direct observation of a suppression of $s\bar{s}$ production from the vacuum with respect to $u\bar{u}$ or $d\bar{d}$ production. Assuming *all* $K^\pm$ in the range $x_p > 0.5$ to be leading, we calculate $\gamma_s = 0.25 \pm 0.03$, consistent with values [25] derived from inclusive measurements of the relative production rates of strange and non-strange,

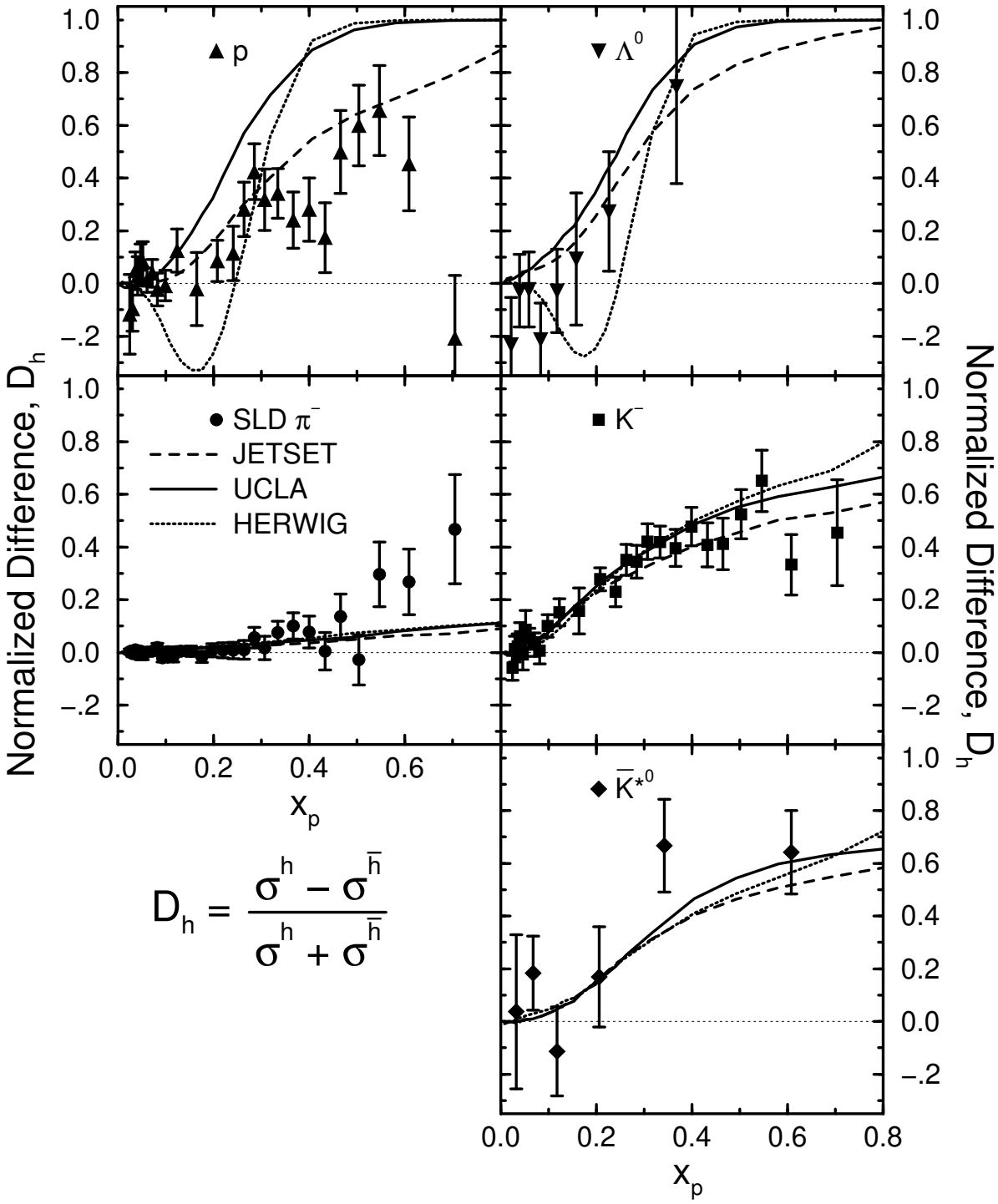

Figure 10: Normalized production differences between hadrons and their respective antihadrons in light quark jets. Also shown are the predictions of three fragmentation models.

pseudoscalar and vector mesons.

Also shown in fig. 10 are the predictions of the three Fragmentation models. All three are consistent with the meson data and with the Λ^0 data. The JETSET model is also consistent with the proton data, however the other two models predict a saturated value of $D_{\rm p}$ for $x_p > 0.4$ that is inconsistent with the data.

7 Summary and Conclusions

Using the SLD Cherenkov Ring Imaging Detector we have made preliminary measurements of charged pion, kaon and proton production over most of the momentum range in hadronic Z^0 decays. We find the predictions of the JETSET, UCLA and HERWIG fragmentation models to be in qualitative agreement with our data. We find the predictions of MLLA QCD+LPHD to be consistent with our data over a wide range in the ξ distribution. These results are in agreement with our previous results and those from other experiments.

By isolating high-purity light- and b-flavor samples, we have measured hadron production in light-flavor events, as well as in c- and b-flavor events. We find substantial differences in particle production between light- and heavy-flavor events, with the latter producing more mesons overall, but far fewer at high momentum. These qualitative features are expected given the hard fragmentation and high average decay multiplicity of heavy hadrons. The light-flavor sample is more suitable for testing predictions of QCD that assume massless quarks, as well as for testing fragmentation models. We find differences between fragmentation model predictions and our data similar to those found in the inclusive sample, indicating that the deficiencies lie in the simulation of fragmentation rather than in that of heavy hadron production and decay.

By isolating a high-purity gluon jet samples, and comparing with a mixture of light-quark and gluon jets, we have tested the hypothesis that the relative production of charged stable hadrons is the same in light quark and glkuon jets. We observe deviations from equality consistent with those predicted by our simulation to arise from kinematic biases in the jet selection, and conclude that the hypothesis of equality is satisfied to within a few percent.

By isolating high-purity light-quark and light-antiquark samples, we have made the first comparison of hadron and antihadron production in light-quark jets in e^+e^- annihilation. We observed an excess of p over $\bar{\rm p}$, which appears to increase with momentum, and provides direct evidence for the "leading particle" hypothesis that high momentum protons are more likely to contain the primary quark. We also observed a large excess of high momentum K^- over K^+ indicating that a high momentum kaon is likely to contain a primary quark or antiquark from the Z^0 decay, and that leading kaons are produced predominantly in $s\bar{s}$ events rather than $d\bar{d}$ or $u\bar{u}$ events. We observe a smaller excess of π^- over π^+ at high momentum, consistent with expectations assuming equal and opposite signals from $u\bar{u}$ and $d\bar{d}$ events.

Acknowledgements

We thank the personnel of the SLAC accelerator department and the technical staffs of our collaborating institutions for their outstanding efforts on our behalf. This work was supported by the U.S. Department of Energy, the UK Particle Physics and Astronomy Research Council (Brunel, Oxford and RAL); the Istituto Nazionale di Fisica Nucleare of Italy (Bologna, Ferrara, Frascati, Pisa, Padova, Perugia); the Japan-US Cooperative Research Project on High Energy Physics (Nagoya, Tohoku); and the Korea Science and Engineering Foundation (Soongsil).

References

[1] T.I. Azimov, Y.L. Dokshitzer, V.A. Khoze, S.I. Troyan, Z. Phys. **C27** (1985) 65.

[2] See e.g. I.G. Knowles and G.D. Lafferty, J. Phys. **G23** (1997) 731.

[3] SLD Design Report, SLAC-Report 273, (1984).

[4] SLD Collaboration: K. Abe et al., Phys. Rev. **D51** (1995) 962.

[5] M.D. Hildreth *et al.*, Nucl. Inst. Meth. **A367** (1995) 111.

[6] C. J. S. Damerell *et al.*, Nucl. Inst. Meth. **A400** (1997) 287.

[7] K. Abe, *et al.*, Nucl. Inst. Meth. **A343** (1994) 74.

[8] SLD Collab., K. Abe *et al.*, Phys. Rev. **D59** (1999) 52001.

[9] S. Brandt *et al.*, Phys. Lett. **12** (1964) 57;
E. Farhi, Phys. Rev. Lett. **39** (1977) 1587.

[10] D. Axen et al., Nucl. Inst. Meth. **A328** (1993) 472.

[11] D.J. Jackson, Nucl. Inst. Meth. **A388** (1997) 247.

[12] T. Sjöstrand, Comp. Phys. Comm. **82** (1994) 74.

[13] P. N. Burrows, Z. Phys. **C41** (1988) 375.
OPAL Collaboration, M.Z. Akrawy et al., Z. Phys. **C47** (1990) 505.

[14] SLD Collaboration, K. Abe et al., Phys. Rev. Lett. **79** (1997) 590.

[15] R. Brun et al., Report No. CERN-DD/EE/84-1 (1989).

[16] K. Abe, *et al.*, Nucl. Inst. and Meth. **A371** (1996) 195

[17] DELPHI Collab., P. Abreu *et al.*, Nucl. Phys. **B444** (1995) 3.

[18] OPAL Collab., P.D. Acton *et al.*, Z. Phys. **C63** (1994) 181.

[19] ALEPH Collab., D. Buskulic *et al.*, Z. Phys. **C66** (1995) 355.

[20] S. Chun and C. Buchanan, Phys. Rep. **292** (1998) 239.

[21] G. Marchesini *et al.*, Comp. Phys. Comm. **67** (1992) 465.

[22] Particle Data Group, Phys. Rev. **D54** (1996) 1.

[23] H.J. Kang, Ph. D Thesis, Rutgers University, November 2001; SLAC-Report-590.

[24] SLD Collab., K. Abe *et al.*, Phys. Rev. Lett. **78** (1997) 3442.

[25] D.H. Saxon, *High Energy Electron-Positron Physics*, Eds. A. Ali and P. Söding, World Scientific (1988), p. 539.

**List of Authors

Koya Abe,[24] Kenji Abe,[15] T. Abe,[21] I. Adam,[21] H. Akimoto,[21] D. Aston,[21] K.G. Baird,[11] C. Baltay,[30] H.R. Band,[29] T.L. Barklow,[21] J.M. Bauer,[12] G. Bellodi,[17] R. Berger,[21] G. Blaylock,[11] J.R. Bogart,[21] G.R. Bower,[21] J.E. Brau,[16] M. Breidenbach,[21] W.M. Bugg,[23] D. Burke,[21] T.H. Burnett,[28] P.N. Burrows,[17] A. Calcaterra,[8] R. Cassell,[21] A. Chou,[21] H.O. Cohn,[23] J.A. Coller,[4] M.R. Convery,[21] V. Cook,[28] R.F. Cowan,[13] G. Crawford,[21] C.J.S. Damerell,[19] M. Daoudi,[21] S. Dasu,[29] N. de Groot,[2] R. de Sangro,[8] D.N. Dong,[13] M. Doser,[21] R. Dubois, I. Erofeeva,[14] V. Eschenburg,[12] E. Etzion,[29] S. Fahey,[5] D. Falciai,[8] J.P. Fernandez,[26] K. Flood,[11] R. Frey,[16] E.L. Hart,[23] K. Hasuko,[24] S.S. Hertzbach,[11] M.E. Huffer,[21] X. Huynh,[21] M. Iwasaki,[16] D.J. Jackson,[19] P. Jacques,[20] J.A. Jaros,[21] Z.Y. Jiang,[21] A.S. Johnson,[21] J.R. Johnson,[29] R. Kajikawa,[15] M. Kalelkar,[20] H.J. Kang,[20] R.R. Kofler,[11] R.S. Kroeger,[12] M. Langston,[16] D.W.G. Leith,[21] V. Lia,[13] C. Lin,[11] G. Mancinelli,[20] S. Manly,[30] G. Mantovani,[18] T.W. Markiewicz,[21] T. Maruyama,[21] A.K. McKemey,[3] R. Messner,[21] K.C. Moffeit,[21] T.B. Moore,[30] M. Morii,[21] D. Muller,[21] V. Murzin,[14] S. Narita,[24] U. Nauenberg,[5] H. Neal,[30] G. Nesom,[17] N. Oishi,[15] D. Onoprienko,[23] L.S. Osborne,[13] R.S. Panvini,[27] C.H. Park,[22] I. Peruzzi,[8] M. Piccolo,[8] L. Piemontese,[7] R.J. Plano,[20] R. Prepost,[29] C.Y. Prescott,[21] B.N. Ratcliff,[21] J. Reidy,[12] P.L. Reinertsen,[26] L.S. Rochester,[21] P.C. Rowson,[21] J.J. Russell,[21] O.H. Saxton,[21] T. Schalk,[26] B.A. Schumm,[26] J. Schwiening,[21] V.V. Serbo,[21] G. Shapiro,[10] N.B. Sinev,[16] J.A. Snyder,[30] H. Staengle,[6] A. Stahl,[21] P. Stamer,[20] H. Steiner,[10] D. Su,[21] F. Suekane,[24] A. Sugiyama,[15] A. Suzuki,[15] M. Swartz,[9] F.E. Taylor,[13] J. Thom,[21] E. Torrence,[13] T. Usher,[21] J. Va'vra,[21] R. Verdier,[13] D.L. Wagner,[5] A.P. Waite,[21] S. Walston,[16] A.W. Weidemann,[23] E.R. Weiss,[28] J.S. Whitaker,[4] S.H. Williams,[21] S. Willocq,[11] R.J. Wilson,[6] W.J. Wisniewski,[21] J.L. Wittlin,[11] M. Woods,[21] T.R. Wright,[29] R.K. Yamamoto,[13] J. Yashima,[24] S.J. Yellin,[25] C.C. Young,[21] H. Yuta.[1]

[1] *Aomori University, Aomori, 030 Japan,*
[2] *University of Bristol, Bristol, United Kingdom,*
[3] *Brunel University, Uxbridge, Middlesex, UB8 3PH United Kingdom,*
[4] *Boston University, Boston, Massachusetts 02215,*
[5] *University of Colorado, Boulder, Colorado 80309,*
[6] *Colorado State University, Ft. Collins, Colorado 80523,*

[7] *INFN Sezione di Ferrara and Universita di Ferrara, I-44100 Ferrara, Italy,*
[8] *INFN Laboratori Nazionali di Frascati, I-00044 Frascati, Italy,*
[9] *Johns Hopkins University, Baltimore, Maryland 21218-2686,*
[10] *Lawrence Berkeley Laboratory, University of California, Berkeley, California 94720,*
[11] *University of Massachusetts, Amherst, Massachusetts 01003,*
[12] *University of Mississippi, University, Mississippi 38677,*
[13] *Massachusetts Institute of Technology, Cambridge, Massachusetts 02139,*
[14] *Institute of Nuclear Physics, Moscow State University, 119899 Moscow, Russia,*
[15] *Nagoya University, Chikusa-ku, Nagoya, 464 Japan,*
[16] *University of Oregon, Eugene, Oregon 97403,*
[17] *Oxford University, Oxford, OX1 3RH, United Kingdom,*
[18] *INFN Sezione di Perugia and Universita di Perugia, I-06100 Perugia, Italy,*
[19] *Rutherford Appleton Laboratory, Chilton, Didcot, Oxon OX11 0QX United Kingdom,*
[20] *Rutgers University, Piscataway, New Jersey 08855,*
[21] *Stanford Linear Accelerator Center, Stanford University, Stanford, California 94309,*
[22] *Soongsil University, Seoul, Korea 156-743,*
[23] *University of Tennessee, Knoxville, Tennessee 37996,*
[24] *Tohoku University, Sendai, 980 Japan,*
[25] *University of California at Santa Barbara, Santa Barbara, California 93106,*
[26] *University of California at Santa Cruz, Santa Cruz, California 95064,*
[27] *Vanderbilt University, Nashville,Tennessee 37235,*
[28] *University of Washington, Seattle, Washington 98105,*
[29] *University of Wisconsin, Madison,Wisconsin 53706,*
[30] *Yale University, New Haven, Connecticut 06511.*